Charged particle transport in antidot lattices in the presence of magnetic and electric fields: Langevin approach

M. Khoury,[1] A. M. Lacasta,[2] J. M. Sancho,[1] A. H. Romero,[3] and Katja Lindenberg[4]
[1]*Departament d'Estructura i Constituents de la Matèria, Facultat de Física, Universitat de Barcelona, Diagonal 647, E-08028 Barcelona, Spain*
[2]*Departament de Física Aplicada, Universitat Politècnica de Catalunya, Avinguda Doctor Marañon 44, E-08028 Barcelona, Spain*
[3]*Cinvestav-Querétaro, Libramiento Norponiente 200, 76230, Fracc. Real de Juriquilla, Querétaro, Querétaro, Mexico*
[4]*Department of Chemistry and Biochemistry 0340, and Institute for Nonlinear Science, University of California San Diego, La Jolla, California 92093-0340, USA*
(Received 30 July 2008; revised manuscript received 10 September 2008; published 28 October 2008)

Magnetotransport experiments on antidot lattices show a rich variety of physical phenomena. Depending on the value of the particle mean-free path l in relation to the period λ of regular scatterers, two very different regimes can be distinguished: the strongly diffusive ($l \ll \lambda$) and the weakly diffusive ($l \gtrsim \lambda$). We study particle transport in two-dimensional periodic landscapes based on a classical Langevin equation. The model covers both regimes and exhibits many of the features found experimentally at low magnetic fields. The most interesting observation is the presence of anomalous peaks in the magnetoresistance as a function of the magnetic field in the weakly diffusive regime. The roles of finite temperatures and of the electric field are also discussed.

DOI: 10.1103/PhysRevB.78.155433 PACS number(s): 73.23.−b, 05.40.−a, 73.40.−c

I. INTRODUCTION

Interesting mesoscopic experiments in semiconductors have been carried out in two-dimensional (2D) electron gases (2DEG) formed at the interface between two semiconductors with different band gaps (typically *n*-type AlGaAs and *p*-type GaAs).[1] When these semiconductors are brought in contact, they form a heterojunction whose energy bands are different from the valence and conduction bands of the individual semiconductors. Electron transfer takes place from the semiconductor with the wider band gap (*n* AlGaAs) to the other, leaving behind some positive donors. This charged zone produces an electrostatic potential that causes the bands to bend at the interface, forming a triangular potential well where the Fermi energy E_F (which is constant everywhere at equilibrium) remains inside the conduction band. At low temperatures, the electric current is carried mainly by electrons whose energy is close to the Fermi energy so they remain trapped in this region, being free to move in two dimensions but tightly confined in the third (the direction perpendicular to the interface).[1]

This very thin conducting layer is called a 2DEG and appears in many transistorlike structures. It represents a high mobility system which offers the possibility of exploring the fundamental physics of electron transport. Charge density in this type of system can be spatially modulated by imposing a confining potential by means of conventional fabrication techniques. For example, lithography can be used to fabricate a modulated array of holes on a surface which can then be transferred to the 2DEG by deep mesa etching.[2,3]

Most attention has been focused on periodic modulations. Depending on the amplitude of this modulation in relation to the Fermi energy, the structure can be an array of quantum dots (in which electrons are confined) or, if these dots overlap, an array of voids or "antidots" (regions impenetrable to the electrons). Moreover, using appropriate experimental techniques, it is possible to reduce the depletion region around each antidot (i.e., the region from which the carriers have diffused away). As a result, it is possible to obtain weak saddle points between antidots, that is, an essentially flat surface with a steep obstacle landscape. This configuration appears to be optimal in exhibiting interesting "anomalous" phenomena.

A different but conceptually related class of transport experiments that are receiving increasing interest involves paramagnetic colloidal particles on patterned surfaces driven by applied magnetic fields. Here the observations include sorting of particles of different characteristics such as size, directed transport, and anomalous diffusion.[4]

An inclusive approach to these types of problems leads us to focus on transport properties of charged particles through antidot arrays at low magnetic fields. Standard four-terminal magnetoresistance measurements (see Fig. 1 in Ref. 5) show an oscillatory dependence of the magnetoresistance on the magnetic field B (see Fig. 2 in Ref. 6, arguably the paradigmatic reference on commensurability effects in antidot arrays). These oscillations reveal a dependence on the period of the imposed pattern,[3,5–10] and differ from the well-defined Shubnikov-de Haas oscillations of quantum-mechanical origin associated with time-periodic variations in $1/B$. In our work we explore some of the physical mechanisms that are responsible for the observed phenomena by performing numerical simulations of the particle motion based on classical orbit theory to describe electron dynamics. Our approach of course does not capture quantum effects but it is nevertheless able to capture theoretical and experimental observations over a wide range of values of the particle mean-free path within a single model formulation. Thus, while we cannot aspire to quantitative agreement with quantum experiments, it is interesting that one can capture many of the observed features qualitatively with a classical formulation.

The paper is organized as follows. In Sec. II we introduce the model and specify the observables. In Sec. III we present the numerical simulation results and their comparison with

available theoretical and experimental data. Finally, we end with some conclusions in Sec. IV.

II. MODEL

Most experimental observations[3,5–9] as well as existing theoretical studies[9–12] confirm that transport experiments in modulated 2DEG can be understood at least qualitatively in terms of classical nonlinear dynamics provided that the antidot lattice spacing is larger than the wavelength associated with the typical particle energy (Fermi wavelength in an electron system) and the magnetic field B is not too strong. In this vein, the model we introduce considers a set of independent charged particles moving on a two-dimensional $x-y$ surface covered by a regular array of obstacles, in the presence of crossed electric ($\boldsymbol{E}=E\hat{x}$) and magnetic ($\boldsymbol{B}=B\hat{z}$) fields. In the Langevin framework, the particles are also subject to thermal noise and the associated dissipation. The equations of motion can be written as

$$m\ddot{x} = qB\dot{y} + qE - \frac{\partial V}{\partial x} - \gamma\dot{x} + \xi_x(t),$$

$$m\ddot{y} = -qB\dot{x} - \frac{\partial V}{\partial y} - \gamma\dot{y} + \xi_y(t), \tag{1}$$

where m is the particle mass and q is the particle charge. The friction coefficient γ gives rise to a momentum relaxation time $\tau_\gamma = m/\gamma$, and the $\xi_i(t)$ are mutually uncorrelated white noises that obey the fluctuation-dissipation relation at temperature T,

$$\langle \xi_i(t)\xi_j(t')\rangle = 2\epsilon\delta_{ij}\delta(t-t'), \tag{2}$$

with noise intensity $\epsilon = k_B T\gamma$. A continuous periodic potential is used to model the antidot array,

$$V(x/\lambda, y/\lambda) = V_0 \mathcal{U}(x/\lambda, y/\lambda)$$

$$= \frac{V_0}{1+\exp\left\{-a\left[\cos\left(\frac{2\pi x}{\lambda}\right)+\cos\left(\frac{2\pi y}{\lambda}\right)-2b\right]\right\}}, \tag{3}$$

where λ is the spatial period. The parameter V_0 controls the height of the obstacles, a controls their steepness, and b determines the size of an obstacle relative to the spatial period λ, in such a way that for fixed a, larger values of b lead to shallower and narrower obstacles. Both of these parameters also affect the obstacle height. A finite portion of this potential, and the effect of changing a (b) for fixed b (a), are shown in Fig. 1.

In the absence of the potential ($V_0=0$), a uniform magnetic field B causes the charged particle to perform cyclotron motion on a time scale,

$$t_c = \frac{m}{|q|B}. \tag{4}$$

Measuring time in units of this characteristic time and length in units of the lattice constant leads to scaled variables $r_x = x/\lambda$, $r_y = y/\lambda$, and $s = t/t_c = |q|Bt/m$. Consequently, the equations of motion (1) and the fluctuation-dissipation relation (2) can be rewritten as

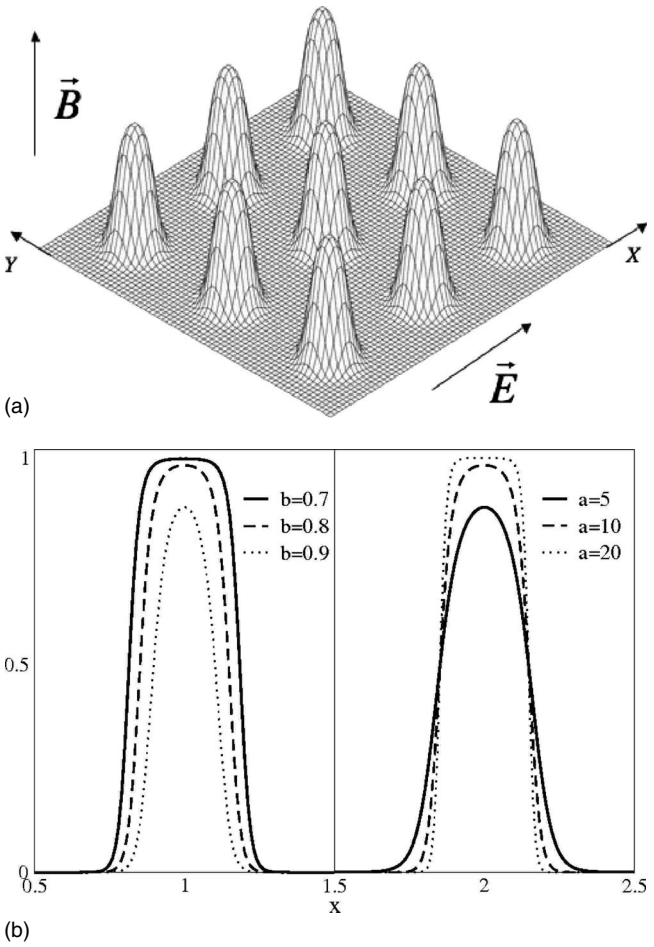

FIG. 1. Upper panel: a finite portion of the two-dimensional periodic potential [Eq. (3)] for parameters $a=5$, $b=0.8$. Lower panel: potential profiles $V(x,0)$ for fixed $a=10$ (left) and fixed $b=0.8$ (right). $V_0=1$ in both panels.

$$\ddot{r}_x = -\dot{r}_y + \frac{\tilde{E}}{B^2} - \frac{\tilde{V}_0}{B^2}\frac{\partial \mathcal{U}}{\partial r_x} - \frac{\tilde{\gamma}}{B}\dot{r}_x + \eta_x(s),$$

$$\ddot{r}_y = \dot{r}_x - \frac{\tilde{V}_0}{B^2}\frac{\partial \mathcal{U}}{\partial r_y} - \frac{\tilde{\gamma}}{B}\dot{r}_y + \eta_y(s), \tag{5}$$

and

$$\langle \eta_i(s)\eta_j(s')\rangle = 2\frac{\tilde{\mathcal{T}}\tilde{\gamma}}{B^3}\delta_{ij}\delta(s-s'), \tag{6}$$

where

$$\tilde{E} = -\frac{mE}{\lambda q}, \quad \tilde{V}_0 = \frac{mV_0}{\lambda^2 q^2}, \quad \tilde{\gamma} = \frac{\gamma}{q}, \quad \tilde{\mathcal{T}} = k_B T\frac{\tilde{V}_0}{V_0}. \tag{7}$$

As can be seen in these equations, the choice of t_c as the characteristic time of the system leads to the explicit display of the dependence of all the terms in the equations of motion

(5) on magnetic field B. This choice differs from the scaling used in other numerical work.[10,11] For qualitative comparison with experimental work and with other existing computer simulations we set the charge q equal to the electronic charge $-\epsilon$ (ϵ being the elementary charge) and m equal to the effective mass of an electron in a 2DEG in the single-particle approximation, i.e., $0.067m_e$ (where m_e is the mass of an electron).

Relation (7) defines the four independent parameters of the model whose values must be fixed in every numerical experiment and related to experimental values. Note that these four redefined parameters are not dimensionless. Indeed, they carry unusual dimensions but allow us to focus on the B dependence of our results. We fix these parameters in our computations and focus on the behavior of the resistivity as a function of the magnetic field.

The standard observables for this scenario are: (1) The diagonal and off-diagonal resistivities ρ_{xx} and ρ_{xy} in a square geometry,

$$\rho_{xx} = \frac{\sigma_{xx}}{\sigma_{xx}^2 + \sigma_{xy}^2} = \frac{-Em}{q^2 B n_s \lambda} \frac{\langle \dot{r}_x \rangle}{[\langle \dot{r}_x \rangle^2 + \langle \dot{r}_y \rangle^2]},$$

$$\rho_{xy} = \frac{\sigma_{xy}}{\sigma_{xx}^2 + \sigma_{xy}^2} = \frac{-Em}{q^2 B n_s \lambda} \frac{\langle \dot{r}_y \rangle}{[\langle \dot{r}_x \rangle^2 + \langle \dot{r}_y \rangle^2]}, \tag{8}$$

which measure the electric response parallel and perpendicular to the applied electric field. The parameter n_s is the charge density in 2D, which is a known quantity in the case of an electronic system. ρ_{xx} is called the magnetoresistance and ρ_{xy} is the Hall resistance. Here we have used the fact that the conductivity tensor $\boldsymbol{\sigma}=\boldsymbol{\rho}^{-1}$ relates the electric field $\boldsymbol{E}$ and the electron velocity vector $\boldsymbol{v}$, $n_s q \boldsymbol{v} = \boldsymbol{\sigma} \boldsymbol{E}$. (2) The resistivity ratio ("rotation number") ρ,

$$\rho = \frac{\rho_{xy}}{\rho_{xx}} = \frac{\langle \dot{r}_y \rangle}{\langle \dot{r}_x \rangle}. \tag{9}$$

In the case of an unpatterned 2DEG, Eq. (5) leads to the resistivity ratio

$$\rho_0 = \frac{Be}{\gamma} = \frac{B}{\tilde{\gamma}} \tag{10}$$

at long times.

We now proceed to obtain these quantities from our numerical simulations as functions of the external parameters B, E, and γ.

III. SIMULATION RESULTS AND DISCUSSION

In a classical approach to charged particle transport, the interaction between the circular trajectories induced by B and the antidot array gives rise to chaotic motion. Together with the stochasticity in the model [Eq. (1)], the problem becomes analytically intractable. Therefore, we have proceeded to perform numerical simulations of the Langevin Eq. (5) using a second-order Runge-Kutta stochastic algorithm.[13]

We consider two different initial conditions. First, in the strongly diffusive regime, the charged particles are initially uniformly distributed over a region between antidots with random initial velocities. Specifically, we place the particles in square regions of size $0.125\lambda \times 0.125\lambda$ centered between obstacles, having ascertained that for all the parameters used in our simulations the ratio $V(x,y)/V_0$ is zero to at least four significant figures in these regions. Second, in the weakly diffusive regime the particles are initially aligned perpendicular to the electric field with a Gaussian distribution of velocity magnitudes whose average is the Fermi velocity ($v_F = 3 \times 10^7$ cm s^{-1} in the case of electrons). This mimics the arrival of particles in the region where the magnetic field is present upon application of an electric field (as happens in an electrode).

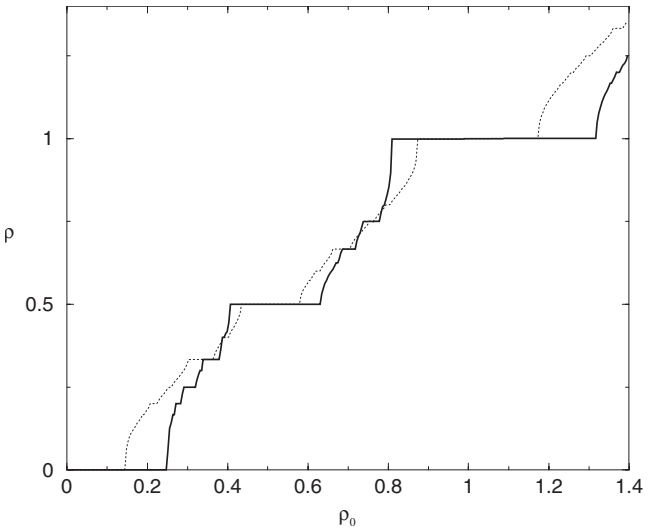

FIG. 2. Resistivity ratio ρ vs the resistivity ratio when $V_0=0$ ($\rho_0 = B/\tilde{\gamma}$) for $\tilde{E}=1.75$, $\tilde{\gamma}=5$, $T=0$ K, and potential parameters: $\tilde{V}_0=0.175$, $a=5$, $b=0.7$ (solid line), and $b=0.9$ (dotted line).

A. Strongly diffusive regime

The charged particle motion is said to be strongly diffusive when the cyclotron frequency becomes irrelevant to the motion. This occurs when the particle mean-free path l (measured in the absence of the periodic potential) is much smaller than the period λ of the regular scatterers, and is thus characterized by rapid momentum relaxation (small τ_γ or large γ). It also requires a sufficiently small obstacle height parameter V_0. There are no experimental results in this regime but we are able to compare our results with those in Ref. 12, also classical, but where the periodic potential is modeled by a cosine product instead of the functional form Eq. (3) proposed in this paper. To facilitate the comparison, in this subsection we set the values $\lambda=0.5$ μm and $n_s = 10^{12}$ cm^{-2} as in Ref. 12. Note that in this regime the results are insensitive to the initial distribution of the particles.

The results exhibited in Figs. 2 and 3 should be viewed in conjunction with the associated trajectories shown in Fig. 4 for a fixed electric field along the x direction. In this overdamped regime the inertial terms in the equations of motion (5) can be neglected ($\ddot{r}_x = \ddot{r}_y = 0$). In the absence of the obstacles the trajectories are straight lines in a direction deter-

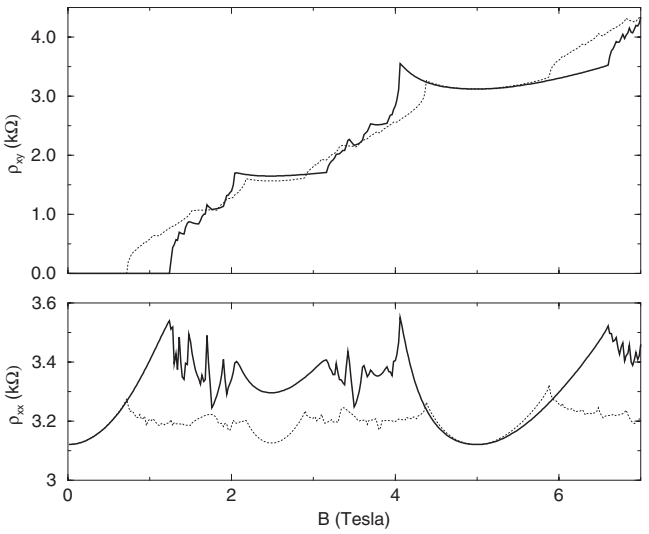

FIG. 3. Hall resistance ρ_{xy} and magnetoresistance ρ_{xx} vs magnetic field B for the same parameters as in Fig. 2.

mined by the magnitude of the perpendicular magnetic field at an angle from the x axis that increases with increasing magnetic-field magnitude B. These are indicated by the dashed lines in the figure. The average velocity components associated with these trajectories in the steady state are found directly from the equations of motion (5) upon setting $\langle \dot{r}_i \rangle = 0$ (in this overdamped regime this state is reached quickly),

$$\langle \dot{r}_x \rangle = \frac{\tilde{\gamma}}{B} \frac{\tilde{E}}{B^2 + \tilde{\gamma}^2}, \quad \langle \dot{r}_y \rangle = \frac{\tilde{E}}{B^2 + \tilde{\gamma}^2}. \tag{11}$$

Note that therefore the trajectories in the figure all have different velocity components and total velocities, even in the absence of obstacles. Also, note that Figs. 2–4 are obtained for zero temperature and hence these average velocities are the actual velocities. For each magnetic-field value we show two trajectories for different values of the parameter b whose increasing value is associated with shallower and narrower obstacles. While the obstacles of course affect the particle velocities, these are again essentially constant in time. Focus, for instance, on the trajectory associated with the lowest magnetic field ($B=1.2$ tesla) and $b=0.7$ (solid line). The important observation is that the particle trajectory in the presence of the obstacles is essentially horizontal due to obstacle avoidance while it evolves at an angle if the obstacles are not there (or if the obstacles are less prominent, $b=0.9$).

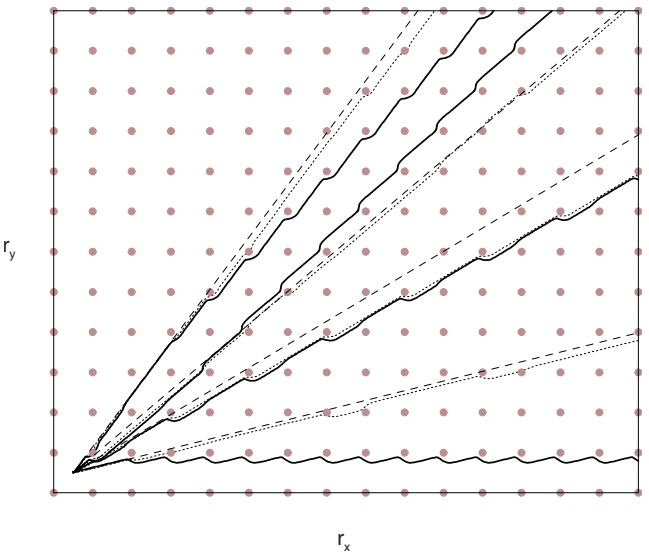

FIG. 4. (Color online) Trajectories for $B=1.2$, 2.9, 4.1, and 6.5 tesla, with increasing angles corresponding to increasing values of B. Results are shown for two different potential parameters, $b=0.7$ (solid lines) and $b=0.9$ (dotted lines). The dashed lines indicate the particle flow direction in the absence of antidots.

Indeed, for any value of the magnetic field below and perhaps somewhat above $B=1.2$ tesla, the trajectory with the more prominent obstacles is essentially horizontal and thus its direction is insensitive to the value of the magnetic field. There are thus ranges of values of the magnetic field for which the obstacles deviate the particle flow toward the x direction and, similarly, some regimes of B values for which the obstacles deviate the flow toward the y direction. One can think of this as the "trapping" of trajectories in the presence of obstacles. As a result, ρ_{xx} vs B exhibit peaks, as can be seen in the bottom panel of Fig. 3. The very same insensitivity to changes in B induced by the obstacles disturbs the otherwise linear ρ_{xy} vs B behavior of the off-diagonal resistivity, leading to the plateaus with dips seen in the upper panel of Fig. 3 and, as a consequence, the plateaus in the resistivity ratio seen in Fig. 2. In Ref. 12 these features are analyzed formally and in detail (for the potential used in that work), and are related to the dynamical phenomenon of mode locking. In particular, it is shown that the plateaus are described as a Devil's staircase. In general, the peaks and plateaus depend on the parameters V_0 and b, and become less pronounced when the obstacles are smaller and narrower, as can be seen in the dotted lines in the figures; as b decreases (larger obstacles) the plateaus become longer. This sort of trajectory trapping behavior has also been seen in the study of the flow of colloidal particles over periodically patterned surfaces, where this trapping behavior is used to sort particles of different characteristics such as particle size.[14–16] Even though we find a good correlation between our results of Figs. 2 and 3 and those in Ref. 12, we find some differences mainly due to the specific differences in the potential functions. Aside from these differences, the main features discussed in Ref. 12 have been obtained in our simulations as well.

The potential strength or intensity parameter V_0 also affects the magnetoresistance measurements. Lowering its value leads to a larger number of smaller plateaus since new trapping trajectories are now possible between those associated with the long plateaus at higher values of V_0.

Another interesting insight provided by our study is the role of temperature. It is clear that as the temperature T increases the trajectories become more erratic and, as a consequence, the magnetoresistance maxima lose intensity (as can be seen in Fig. 5).

In this figure, the potential intensity V_0 is larger than before so the details unveiled in Fig. 3 are now no longer resolved. However, three global maxima of the magnetore-

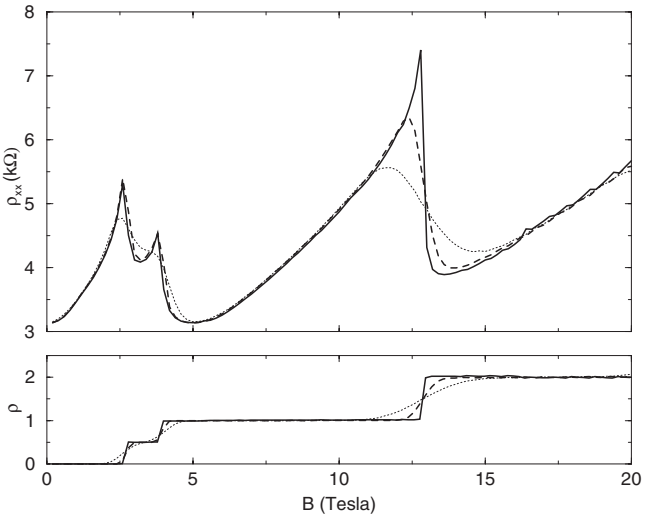

FIG. 5. Magnetoresistance ρ_{xx} (upper panel) and resistivity ratio ρ (lower panel) vs magnetic field extending to high B values for different temperatures. $T=0$ K (solid line), $T=2$ K (dashed line), and $T=20$ K (dotted line). The potential parameters are $\tilde{E}=\tilde{V}_0=1.75$, $a=5$, and $b=0.7$.

sistance are found in the extended B range. Again, they originate from the mechanism discussed earlier.

It is interesting to speculate about the capability of sorting different charged particles with the sort of construct discussed above.[14–16] In this context, one can think of the parameter b as a reflection of the particle characteristics (how the particle "sees" a given array of antidots) such as particle size or electric charge. Thus, a larger value of b would then be associated with a smaller particle. Different particles would then be deflected in different directions by a given magnetic-field intensity, and a mixture of particles could thus be sorted. Figure 6 illustrates the difference in the deflection angles (measured from the x axis defined by the electric-field

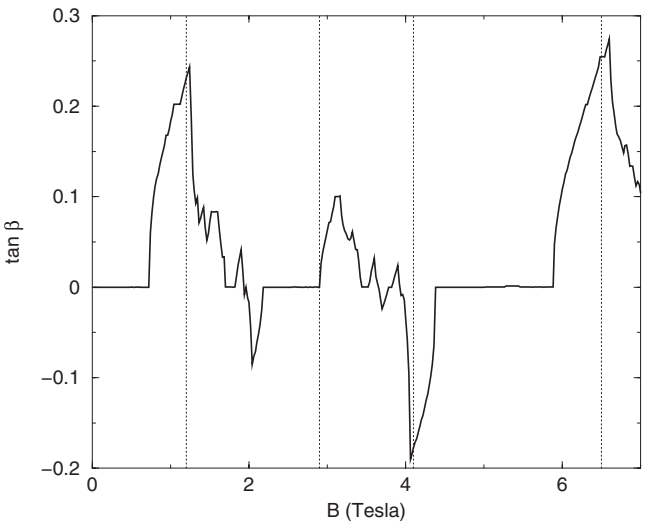

FIG. 6. Comparison of deflection angles for $b=0.7$ and $b=0.9$, calculated in terms of $\beta \equiv \rho(b=0.9)-\rho(b=0.7)$. The dotted lines correspond to the magnetic-field values of the trajectories in Fig. 4. Values of other parameters are as in Fig. 2.

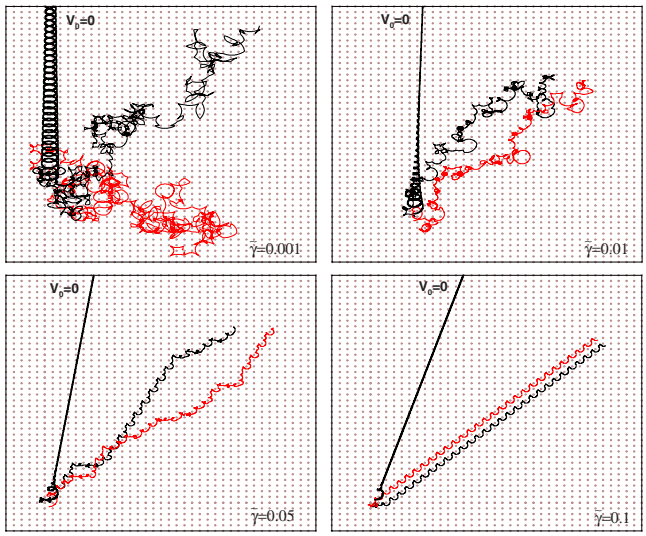

FIG. 7. (Color online) Typical trajectories at $B=0.35$ tesla for different values of the friction parameters indicated in the panels. In each case we include two trajectories in the presence of obstacles, as well as the trajectory in the absence of obstacles. In all panels the remaining parameters are $b=0.7$, $a=5$, $\tilde{E}=0.02$, $\tilde{V}_0=2$, and $T=0$ K.

direction) for two different values of b. This figure reveals the specific B values for optimal sorting for the two values of b chosen in the figure.

B. Weakly diffusive regime

We next move to the regime in which the dissipative interactions between the particles and the environment are weak. It is interesting to characterize the transition from the strongly diffusive to the weakly diffusive regime by considering the typical aspect of trajectories as the friction parameter changes. In Fig. 7 we show typical trajectories for different values of the friction parameter. In each case we also show the trajectory that is followed in the absence of obstacles ($V_0=0$), and we see that in all cases the obstacles cause the particles to move in directions different than that determined by the applied fields alone. At high friction (lower right panel) the trajectories follow the paths described earlier, with deviations from the trajectory in the absence of obstacles (which is a straight line in this regime) caused entirely by collisions with the obstacles. As the friction parameter decreases, the trajectories acquire increasingly chaotic contributions, and we also begin to see the effects of the cyclotron motion both with and without obstacles. At the lowest value of the friction (upper left panel) the trajectories are chaotic and deviate in a random direction from that of the obstacleless case. This latter trajectory clearly exhibits the cyclotron motion contribution.

The weakly diffusive regime considered in this section is thus that illustrated in the upper left panel of Fig. 7. This regime is characterized by a particle mean-free path which is larger than the period of the scatterers, i.e., $l \gtrsim \lambda$. As noted above, in this regime the classical cyclotron motion (with $R_c=mv_F/eB$) becomes relevant to the dynamical description

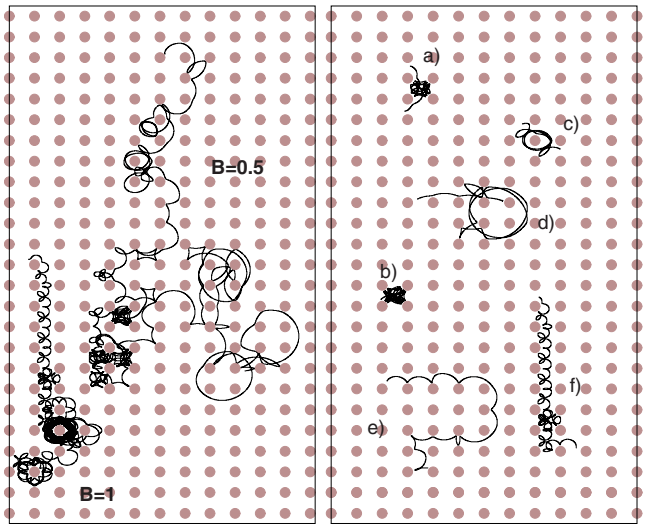

FIG. 8. (Color online) Left panel: single trajectories for two different B values. Right panel: Fragments of single trajectories for different B values. (a) (B=0.5) and (b) (B=0.8) are trapped trajectories, (c) (B=0.5) and (d) (B=0.4) pinned orbits (encircling one and four antidots respectively), and (e) (B=0.6) and (f) (B=1.0) are runaway paths. In both panels the $\tilde{\gamma}$=0.001 and the remaining parameters are as in Fig. 7.

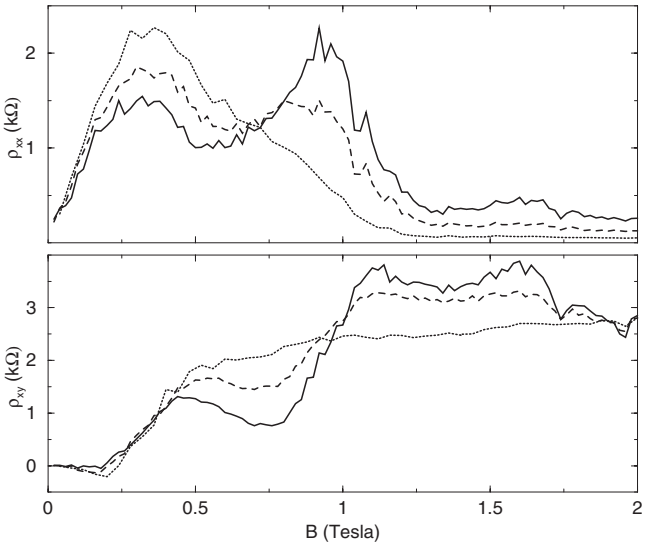

FIG. 9. Magnetoresistance ρ_{xx} and Hall resistance ρ_{xy} vs magnetic field B for $\tilde{\gamma}$=0.001, $\tilde{E}$=0.02, $\tilde{V}_0$=2, T=0 K, a=5, b=0.7, and three different system lengths: L=10 (solid line), L=20 (dashed line), and L=50 (dotted line).

since particles can complete piece-wise circular orbits between collisions with the potential obstacles. This is the regime of existing experiments.[3,5–9] In most experiments λ is in the range of 0.2–0.3 μm and n_s between 1.5×10^{11} and 4.3×10^{11} cm^{-2}, and so we set λ=0.3 μm and n_s=2.4 $\times10^{11}$ cm^{-2} in our simulations (both smaller than in the previous subsection).

It has been claimed in the literature that the most relevant phenomenon in this regime is the occurrence of commensurability peaks in the magnetoresistance, which appear when the potential intensity V_0 is strong (high obstacles) and the magnetic field is very low. These anomalous peaks are not observed in an unpatterned 2DEG. We go on to explore these phenomena.

The (classical) trajectories in the weakly diffusive regime are complicated and have been characterized in a number of different ways, made even more difficult by the fact that in addition to geometry and commensurability there are random thermal contributions, dissipative contributions, and even chaotic contributions to the motion.

On the one hand there are essentially *pinned* or *trapped* orbits (right panel of Fig. 8, fragments c and d) in which the particles either circulate around one or more antidots (with perturbations due to thermal, dissipative, and chaotic contributions) or are trapped within a cell of four obstacles (right panel of Fig. 8, fragments a and b). In these trajectories the particles remain essentially localized and contribute little to the transport process but increase the magnetoresistance.

On the other hand, there are trajectories that are variously called *scattered* or *runaway* in which the particles move along arclike paths from antidot to antidot interrupted by scattering events as they encounter obstacles, which happens more often in the direction perpendicular to the electric field (right panel of Fig. 8, fragments e and f). The precise net direction in which the particles move is a difficult problem that has only been tackled via numerical simulations and experimental observation.[3,5–11] Indeed, in the weakly diffusive regime inertial contributions are important, and each feature of the potential landscape (a, b, and V_0) strongly influences the detailed trajectory and hence the magnetoresistance. For large values of B, a corkscrew or runaway motion in which the charged particles interact very little with the obstacles dominates and, accordingly, there is an increase in the conductance associated with a decrease in the magnetoresistance. This motion is described in detail in Ref. 6. While most discussions in the literature tend to neatly separate the different types of trajectories, the illustrations in the left panel of Fig. 8 make it clear that such a separation is unrealistic and that the various types may contribute to a single trajectory. Charged particles follow trajectories, each of which is sometimes pinned, sometimes runaway, and sometimes even chaotic, and the end result is clearly extremely complex. Indeed, the complexity of the problem makes a quantitative description and comparison with other studies difficult but it does allow for qualitative comparisons of the interesting behaviors observed in this regime where such results are available.

In order to study this complex regime, it is useful to distinguish two possible experimental setups: small systems[5] and large systems.[6] System size is a way to probe different temporal regimes. Accordingly we have performed numerical simulations for three different square lattices of sides L =10, 20, and 50 units of length.

In the smaller lattice (L=10), a rich structure emerges where the magnetoresistance now exhibits two distinct peaks (Fig. 9) that arise from the different ways in which orbitals can become trapped around the potential maxima. Moreover, the details of the results are sensitive to initial condition. That is, the system is underdamped and the particles exhibit important inertial contributions throughout their history.

As the system size is increased, the particles require more time to cover the potential region; the second peak in the magnetoresistance loses intensity ($L=20$), and for an even larger lattice ($L=50$) only one maximum remains, as seen in Fig. 9. This larger B peak is associated with the commensurability relation $R_c \simeq \lambda/2$ and is caused by mostly pinned trajectories. It loses its intensity as the potential landscape becomes steeper, i.e., as the antidot radius shrinks and the saddle points between antidots become weaker (causing interobstacle regions to become flatter). As the effects of the potential weaken in this way, trapping events due to pinned orbits become less probable and runaway trajectory contributions acquire larger x components. In this case ($L=50$) the magnetoresistance as a function of B shows no significant dependence on initial condition.

Our numerical results in both of these low damping regimes are in qualitative and even semiquantitative agreement with experimental outcomes in both Fig. 2 and Table I of Ref. 6, where samples are briefly illuminated, causing the charge-carrier density n_s and the mean-free path l to increase and the effective antidot diameter to decrease.[17] As a consequence, a rich peak structure of lower intensity emerges. In particular in that work the magnetoresistance also exhibits one or two peaks depending on the values of the parameters. However, it is not straightforward to compare quantitatively the curves of Fig. 2 of Ref. 6 with our Fig. 9. In the experimental work, the electrons are quantum-mechanical entities that interact with one another, and therefore a change in n_s, the charge density, does not simply produce a curve shift as it does in our noninteracting classical particle model, e.g., in our Eq. (8). Our only tunable control parameter is the friction, which may reflect particle-phonon interaction effects. The best we can do is to explore whether we can choose this parameter so as to recover the results obtained for a given set of experimental parameters. Indeed, the locations of the magnetoresistance peaks in Fig. 9 and those of Fig. 2 of Ref. 6 are compatible, and correspond to the commensurability conditions $R_c \simeq \lambda/2$ and $R_c \simeq 3\lambda/2$. The irregularity of our peaks results from the fact that, as illustrated in the left panel of Fig. 8, the charged particles follow a highly irregular and even chaotic path, sometimes "quasipinned" and sometimes "quasirunaway."[8] The mechanism of trapping (and consequently the decrease in particles transport) is therefore due to a complex combination of these two types of trajectories. We are thus able to choose parameters that lead to concordance with experimental results. In any case, the long-time behavior as expressed in our largest system always exhibits a single peak in the magnetoresistance due to the dominance of runaway trajectories.

Lastly, we comment on the Hall resistance shown in the lower panel of Fig. 9, and note its qualitatively similar plateau structure (albeit in a different magnetic-field regime) to its behavior in the strongly diffusive case (upper panel of Fig. 3). This is evidence of the fact that even when the trajectories are more complex, there are still ranges of B values for which these now more complex trajectories are pushed by the obstacles to lie along a particular direction, with a resulting directional insensitivity to the value of B. In other words, we see again the "trapping of trajectories" effects on the more complex trajectories caused by the obstacles as observed earlier for the simpler trajectories.

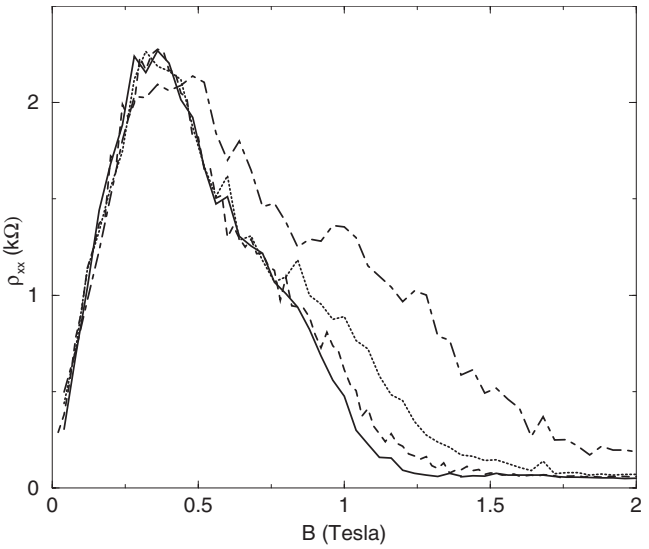

FIG. 10. Resistivity ρ_{xx} vs magnetic field B for different temperatures: $T=0$ K (solid line), $T=10$ K (dashed line), $T=30$ K (dotted line), and $T=100$ K. System size is $L=50$ and parameters are $\tilde{\gamma}=0.001$, $\tilde{E}=0.02$, $\tilde{V}_0=2$, $a=5$, and $b=0.7$.

Our model also allows us to study the dependence of the magnetoresistance on other experimental variables such as the temperature and the electric field, leading to a series of predictions to compare with future experiments. For instance, magnetoresistance experiments are usually performed at very low temperatures (typically $T \lesssim 5$ K), which suppresses the presence of impurities and phonon scattering, but if the sample is of very good quality one should be able to observe the peak broadening typically caused by thermal motion.

Figure 10 reveals that the position of the prominent peak in the magnetoresistance (associated with the commensurability relation $R_c \sim \lambda/2$) is rather insensitive to temperature, and that only for very high temperatures does the curve spread and the position of the magnetoresistance maximum move to slightly higher values of B. Although one may observe other possible small maxima for large B, intrinsic data fluctuations inhibit satisfactory resolution of such peaks.

Finally, the effects of the electric field merit at least preliminary attention. As far as we know, this is a topic not addressed in the literature.

In Fig. 11 we plot the magnetoresistance for several values of the electric field in the small and large system cases. For a small system (upper panel of Fig. 11) both peaks spread and move to the right with increasing field. Surprisingly, for small systems a third peak appears for $B > 1.5$. It is not evident why trajectories become trapped at these values of B but they clearly do. For a large system, the single peak also moves to the right and the B domain of very large magnetoresistance increases (lower panel of Fig. 11).

Figure 12 shows the magnetoresistance as a function of electric field in large systems for three values of the magnetic field within the B scale shown in Fig. 11. We have included ρ_{xx} vs $\tilde{E}$ for values of the electric field smaller than those in Fig. 11 to test if the behavior is in the linear-response regime. Clearly, although small, these electric fields are still not suf-

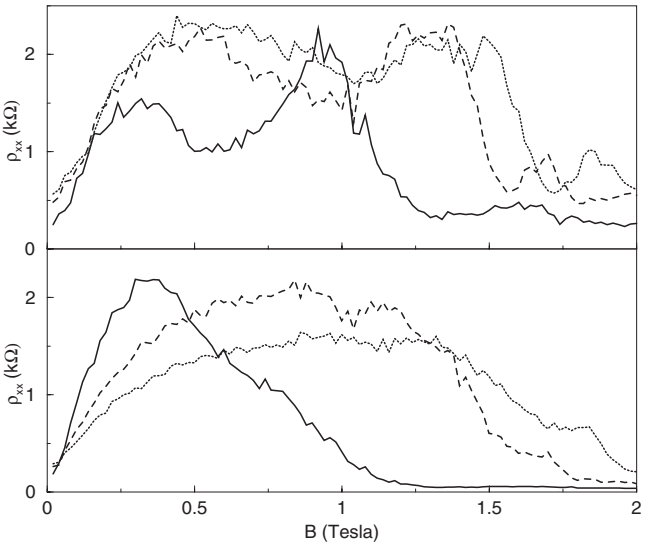

FIG. 11. Magnetoresistance in small (top) and large (bottom) systems for different $\tilde{E}$ values: 0.02 (solid line), 0.07 (dashed line), and 0.1 (dotted line). $T=0$ K; system parameters are the same as in previous figure.

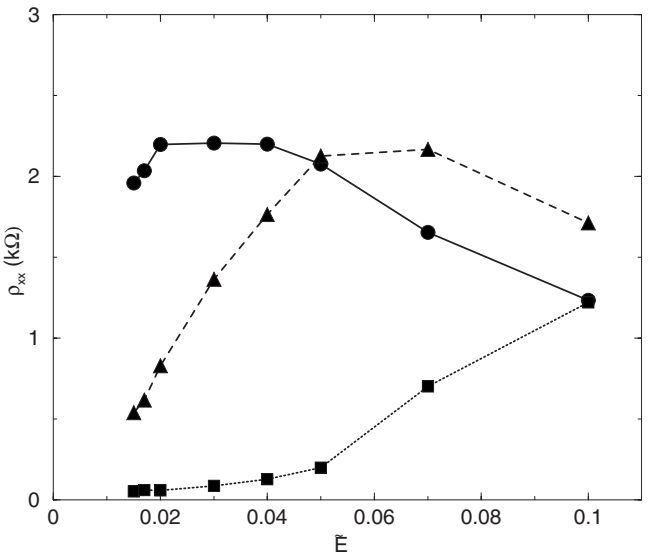

FIG. 12. Magnetoresistance ρ_{xx} vs $\tilde{E}$ for three different B values: 0.35 (solid line), 0.85 (dashed line), and 1.5 tesla (dotted line). The lines simply connect the computed values. System size is $L=50$ and parameters are: $\tilde{\gamma}=0.001$, $\tilde{V}_0=2$, $T=0$ K, $a=5$, and $b=0.7$.

ficiently small to place the system in the linear-response regime where ρ_{xx} is independent of E, except perhaps for the largest B field and the smallest E fields shown. We have not gone to even smaller values of E because the calculations become onerous as it takes a very long time for the particles to cross the system (we have not done this for a small system so as not to obscure the situation with system size effects). These preliminary numerical results exhibiting fairly complex nonlinear behavior will hopefully stimulate new experiments.

IV. CONCLUSIONS

We have modeled magnetotransport phenomena on antidot lattices using a Langevin equation model of classical noninteracting charged particles moving in a two-dimensional spatially modulated potential surface in the presence of external electric and magnetic fields. Our approach is in the spirit of earlier classical approaches to the problem.[8–11] However, our main goal has been to capture the two dynamical regimes that have been studied, the strongly diffusive and the weakly diffusive, within a single model formulation. These have in the past been studied separately.[6,12] Moreover, our model includes a noise term which allows us to explore the temperature dependence of the dynamics and of the magnetoresistance and Hall resistivity.

Our results are consistent with existing results in the strongly diffusive regime (all theoretical).[12] Experiments have all been performed in the weakly diffusive regime,[3,5–9] and our results are qualitatively and even quantitatively consistent with these as well.[6] We have noted the sorting capability of antidot arrays, a capability that has not yet been experimentally pursued. Also, while we have assumed that the electric field E is small, our approach allows us to explore more broadly the role of this parameter in the dynamics as well as the role of temperature. Finally, it is worth stressing again that our parametrization [Eq. (7)] highlights the relevance of cyclotron motion not only in the small B-weakly diffusive regime but also in situations in which particles do not describe closed orbits.

While our model is classical and therefore inherently limited in its ability to capture quantum behavior in a GaAs/GaAlAs systems, we have seen that the model nevertheless does well. A more quantitative test would be possible if there were experiments of this type involving, for instance, charged colloidal particles. While sorting experiments involving uncharged colloids are available, we have not identified any involving charged particles. Perhaps this work will motivate such experiments.

ACKNOWLEDGMENTS

We acknowledge support from Ministerio de Educación y Ciencia (Spain) under Project No. FIS2006-11452 (A.M.L. and J.M.S.) and Grant No. FPU-AP2005-4765 (M.K.). A.H.R. acknowledges the support of Conacyt-Mexico under Project No. J-59853-F.

[1] S. Datta, *Electronic Transport in Mesoscopic Systems* (Cambridge University Press, Cambridge, 1995).
[2] K. Ensslin and R. Schuster, *Fabrication and Electronic Properties of Antidot Superlattices*, III-V Quantum System Research, edited by K. H. Ploog (Institution of Electrical Engineers, United Kingdom, 1995), Chap. 4.
[3] D. Weiss, P. Grambow, K. von Klitzing, A. Menschig, and G. Weimann, Appl. Phys. Lett. **58**, 2960 (1991).
[4] See more references in A. Soba, P. Tierno, T. M. Fischer, and F. Sagués, Phys. Rev. E **77**, 060401(R) (2008).
[5] R. Schuster, K. Ensslin, D. Wharam, S. Kuhn, J. P. Kotthaus, G. Bohm, W. Klein, G. Trankle, and G. Weimann, Phys. Rev. B **49**, 8510 (1994).
[6] D. Weiss, M. L. Roukes, A. Menschig, P. Grambow, K. von Klitzing, and G. Weimann, Phys. Rev. Lett. **66**, 2790 (1991).
[7] F. Nihey and K. Nakamura, Physica B **184**, 398 (1993).
[8] R. Schuster, G. Ernst, K. Ensslin, M. Entin, M. Holland, G. Bohm, and W. Klein, Phys. Rev. B **50**, 8090 (1994).
[9] J. Rychen, T. Vancura, T. Heinzel, R. Schuster, and K. Ensslin, Phys. Rev. B **58**, 3568 (1998).
[10] R. Fleischmann, T. Geisel, and R. Ketzmerick, Phys. Rev. Lett. **68**, 1367 (1992).
[11] T. Nagao, J. Phys. Soc. Jpn. **64**, 4097 (1995).
[12] J. Wiersig and K.-H. Ahn, Phys. Rev. Lett. **87**, 026803 (2001); Physica E (Amsterdam) **12**, 256 (2002).
[13] J. García-Ojalvo and J. M. Sancho, *Noise in Spatially Extended Systems* (Springer, New York, 1999).
[14] P. T. Korda, M. B. Taylor, and D. G. Grier, Phys. Rev. Lett. **89**, 128301 (2002); A. Gopinathan and D. G. Grier, *ibid.* **92**, 130602 (2004); M. P. MacDonald, G. C. Spalding, and K. Dholakia, Nature (London) **426**, 421 (2003); K. Dholakia, G. Spalding, and M. MacDonald, Phys. World **15**, 31 (2002); D. G. Grier, Nature (London) **424**, 810 (2003); L. R. Huang, E. C. Cox, R. H. Austin, and J. C. Sturm, Anal. Chem. **75**, 6963 (2003); L. R. Huang, E. C. Cox, R. H. Austin, and J. C. Sturm, Science **304**, 987 (2004).
[15] A. M. Lacasta, J. M. Sancho, A. H. Romero, and K. Lindenberg, Phys. Rev. Lett. **94**, 160601 (2005); J. M. Sancho, M. Khoury, K. Lindenberg, and A. M. Lacasta, J. Phys.: Condens. Matter **17**, S4151 (2005); J. P. Gleeson, J. M. Sancho, A. M. Lacasta, and K. Lindenberg, Phys. Rev. E **73**, 041102 (2006).
[16] In our earlier work (Ref. 15) on separation of particles flowing over a patterned surface, the quantities equivalent to ρ_{xx} and ρ_{xy} were called the "deflection angle" α and the "absolute velocity angle" Ψ, respectively.
[17] In selectively doped AlGaAs-GaAs heterostructures, a persistent increase in the two-dimensional electron density is observed at T below 150 K if the device is illuminated with infrared or visible light. This process increases both the carrier density and the mobility at low temperatures (Ref. 18).
[18] R. J. Nelson, Appl. Phys. Lett. **31**, 351 (1977).